Intense Wave Formation from Multiple Soliton Fusion and the Role of Extra Dimensions

Feifei Xin[1,2,*] Ludovica Falsi,[1] Davide Pierangeli,[1,3] Fabrizio Fusella,[1] Galina Perepelitsa,[4]
Yehudit Garcia,[4] Aharon J. Agranat,[4] and Eugenio DelRe[1,3]

[1]*Dipartimento di Fisica, Università di Roma "La Sapienza," 00185 Rome, Italy*
[2]*College of Physics and Materials Science, Tianjin Normal University, 300387, Tianjin, China*
[3]*ISC-CNR, Università di Roma "La Sapienza," 00185 Rome, Italy*
[4]*The Brojde Center for Innovative Engineering and Computer Science, The Hebrew University, Jerusalem 91904, Israel*

We experimentally and numerically explore the role of dimensionality in multiple (three or more) soliton fusion supported by nonreciprocal energy exchange. Three-soliton fusion into an intense wave is found when an extra dimension, with no broken inversion symmetry, is involved. The phenomenon is observed for $2+1$D spatial waves in photorefractive crystals, where solitons are supported by a spatially local saturated Kerr-like self-focusing and fusion is driven by the leading nonlocal correction, the spatial analog of the nonlinear Raman effect.

One of the underlying themes of present scientific endeavor is identifying the basic laws that govern systems in which multiple bodies interact and complexity arises [1]. In wave systems, particlelike dynamics emerge when nonlinearity supports solitons, localized waves that bounce, spiral, and interact [2–12]. As their mechanical counterparts, strongly interacting solitons also give rise to complexity-driven phenomena, such as the transition to turbulence [13–18] in soliton gases [19,20], replica symmetry breaking in systems dominated by disorder [21,22], and the formation of rogue waves, a still unsolved puzzle in many-body wave physics.

Rogue waves are statistically rare extreme amplitude perturbations that emerge from an otherwise randomly fluctuating environment. At present, there is no consensus on their origin, the commonly accepted view being that they form through a variety of mechanisms, these including spectral filtering and wave condensation [23,24]. In systems dominated by interacting solitons, rogue waves appear to be the product of complex dynamics resulting from collisions [13–15,24–32]. How this occurs at the microscopic level is unclear. Intuitively, high-amplitude waves may form as multiple solitons fuse through nonreciprocal energy transfer, a scenario that fits well numerical studies and available output waveforms [13,25,33–35].

In nonlinear systems like water, optical fibers, and photorefractive crystals, nonreciprocal energy exchange occurs through the so-called nonlinear Raman effect, the leading nonlocal correction to the standard self-phase-modulation Kerr-like nonlinearity [36–40]. In distinction to the Kerr-like component, the Raman interaction is intrinsically insensitive to the relative phase between the mutually coherent colliding solitons, transferring energy from one soliton to the other only on the basis of their relative velocity with respect to an externally fixed direction in time or space. It is this underlying broken inversion symmetry that can cause Raman soliton coupling to act as a microscopic rectifier, an optical Maxwell demon that drives the formation of rogue waves with long-tail statistics [41,42]. For water waves and optical pulses, the Raman effect is the consequence of the broken inversion symmetry associated with the nonreciprocal built-in causality along propagation. In photorefractive crystals, rogue waves are observed forming out of interacting spatial solitons, nonlinear waves in a transverse plane (say, the x, y plane) that evolve along the beam propagation axis (the z axis), obeying a $2+1$D nonlinear Schrödinger equation [32]. Here, the nonreciprocal Raman effect occurs in space and is associated with an applied electric field. In comparison, other soliton-soliton energy exchanging mechanisms, such as Kerr-like effects, are sensitive both to the relative phase and relative intensity of the single interacting solitons, meaning that they can play a role in causing wave condensation and fusion, but not in driving long-tailed statistics through rectification [43,44].

Interestingly, while nonreciprocal energy exchange leads to soliton amplification for two colliding solitons [41,42], it leads to soliton chaos when the colliding solitons are three or more [45]. Since chaos washes out the statistical effects of rectification, it follows that nonreciprocity does not appear to be scalable in the number of colliding solitons, unable hence to offer a microscopic explanation of the extreme and fluctuating amplitudes of rogue waves. In fact, the dynamics of interacting solitons strongly depends on the dimensionality of the system. Since nonreciprocity implies a broken inversion symmetry along one axis (say x axis), multiple soliton collisions in both x and a subspace orthogonal to x, an extra dimension along which they have no Raman

coupling, may play an unexpected and hereto unexplored key role.

In this Letter we demonstrate experimentally and numerically, for the first time, multiple soliton fusion into single amplified waves through nonlinear nonreciprocal energy exchange. The phenomenon is observed for three optical spatial solitons in photorefractive crystal when the collision is able to access an extra dynamical dimension. For a noncollinear collision, the added dimension is a second transverse axis (y) normal to the nonreciprocal energy flux (along x). For collinear cascaded collisions, the added dimension is along the propagation direction (z), and the intense output wave is observed as a result of cascaded two-soliton fusions, that is, when solitons fuse in sequence along propagation.

Experiments are performed in a compositionally disordered photorefractive potassium-lithium-tantalate-niobate ($K_{0.99}Li_{0.01}Ta_{0.60}Nb_{0.40}O_3$) grown through the top-seeded solution method [41,42,45]. The sample is a zero-cut optical quality specimen that measures $L_x = 2.6$ mm, $L_y = 3.4$ mm, $L_z = 1.8$ mm along the x-y-z axes [see Fig. 1(a)]. It has a photorefractive response for visible light associated with deep inband Cu and V impurities, that also give it a slight green coloring. Measurements are carried out with the sample heated above the room-temperature Curie point ($T_C = 292$ K), at $T = T_C + 6$ K in the paraelectric phase. At this temperature the sample has an unperturbed index of refraction $n_0 = 2.3$, a large quasistatic dielectric constant $\epsilon_r \simeq 1.5 \times 10^4$, and an effective quadratic electro-optic coefficient $g_{eff} = g_{11} = 0.14$ m^{4}C^{-2} when the optical polarization is parallel to the externally applied bias electric field $E_0 = V/L_x$, delivered along the x direction. A $\lambda = 532$ nm beam from a doubled Nd:YAG laser (CNI, model: MSL-FN-532–150 mW) is expanded before propagating through a liquid-crystal spatial-light-modulator (SLM). Sandwiched in between two crossed polarizers (POL1 and POL2), the SLM acts as a 1024 by 1280 pixel intensity modulator. Modulation patterns, producing three separate Gaussian-like beams illustrated in the first panels of Figs. 1(b) and 1(c), are sent from a computer to the SLM. The three beams (beams 1, 2, and 3) are then focused by lens F1 (of focal length 75 mm) onto the input facet of the crystal. The lens gives each of the beams a relative transverse velocity $\mathbf{v}_i$ (in the transverse xy plane) that causes them to cross inside the sample.

We investigate two different kinds of soliton collisions: noncollinear three-soliton collision [Fig. 1(b)], and collinear three-soliton collision [Fig. 1(c)]. In the non-collinear three-soliton collision of Fig. 1(b), the velocity of the three beams $\mathbf{v}_1 = (v_{1x}, v_{1y}) = (\mp 26\ \mu\text{m}/1.8\ \text{mm} = \mp 0.014, \pm 45\ \mu\text{m}/1.8\ \text{mm} = \pm 0.025)$, $\mathbf{v}_2 = (\pm 0.028, 0)$, $\mathbf{v}_3 = (\mp 0.014, \pm 0.025)$, are shown in the third panel. The fourth panel depicts the top view (xz plane) of the single collision of the three solitons. Figure 1(c) shows the scheme for the investigation of a collinear three-soliton collision, where dynamics are occurring along the single transverse x direction, as z evolves [$\mathbf{v}_1 = (0.028, 0)$, $\mathbf{v}_2 = (0, 0)$, $\mathbf{v}_3 = (-0.028, 0)$], as shown in the third panel. To transform the triple collision into a cascade of two distinct two-soliton collisions, beam 1 is made to pass through a glass plate placed in between F1 and the sample itself. Refraction through this plate introduces a controllable distance between the beam 2-3 and 1-3 crossing points [see red arrows in the fourth panel of Fig. 1(c)]. The crystal is also illuminated with a background beam (not shown in Fig. 1), an expanded plane wave component from the laser of intensity I_b and polarization orthogonal to the soliton beams and bias field. The background beam undergoes negligible nonlinear dynamics (the associated $g_{12} \ll g_{11}$), and serves to fix the saturation of the nonlinearity [40]. The intensity ratio between the input peak intensity of each beam and the constant background illumination is fixed to $I_p/I_b \simeq 8$. Beam propagation along the z axis is analyzed imaging the input and output facets through an imaging lens (F2, 50 mm focal length) onto a CMOS camera (Thorlabs, DCC1545M).

Experimental results are compared to the numerical simulation of the full 2 + 1D photorefractive beam propagation [40,45,46]. Key to the simulation is the modeling of the cumulative process by which space-charge forms a local
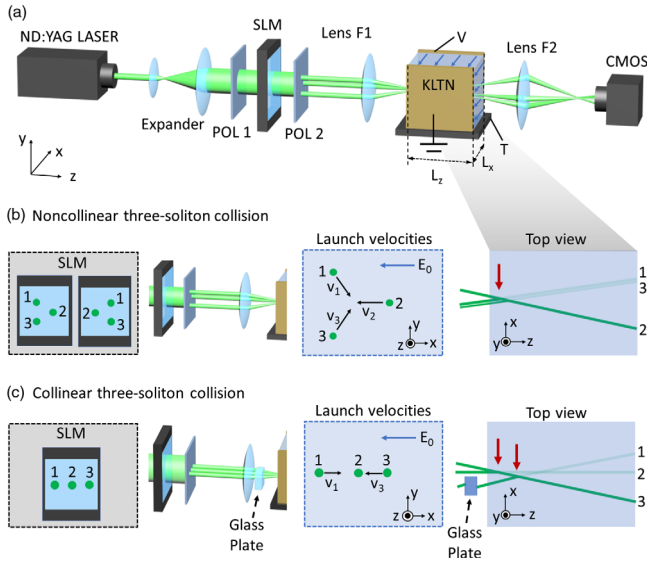

FIG. 1. Three-soliton collision experiments. (a) Experimental setup. (b) Noncollinear three soliton experiment. From left to right: first panel, SLM pattern of modulation that forms the input soliton beams 1, 2, and 3; second panel, beam geometry between SLM and the sample; third panel, input beam transverse velocity; fourth panel, illustration of the collision point (red arrow) in an xz plane top view. (c) Collinear three-soliton experiment. Panels from left to right as above. Note the added glass plate and the now separate collision points (red arrows) of the 2–3 beam and 1–3 beams (fourth panel, see text).
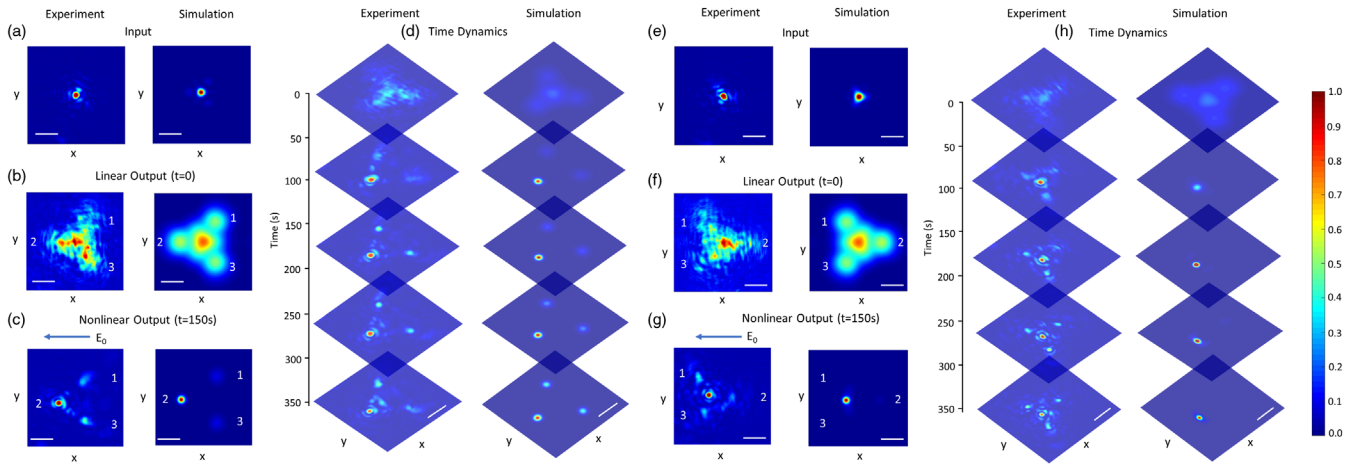
FIG. 2. Noncollinear three-soliton collisions. Observed and simulated intensity distribution at input (a), linear output ($t = 0$) (b), nonlinear output for $t = 150$ s (c), and full time dynamics ($0 < t < 350$ s) (d) for a sample input geometry [first configuration illustrated in inset of Fig. 1(b)]. (e)–(h), corresponding result for a second sample input geometry [second configuration illustrated in inset of Fig. 1(b)]. Note that the final output fused soliton states [panels (c) and (g)] manifest a form of transverse momentum conservation only in the y direction, while no such conservation is found in the x direction, where symmetry is intrinsically broken by the nonreciprocal nature of the energy transfer along the direction of $\mathbf{E}_0$. The scale bar is for 50 μm.

Kerr-like self-focusing component and a nonlocal Raman-like component as a function of exposure time t (see Supplemental Material [47]).

Figure 2 reports results for two paradigmatic noncollinear three-soliton collisions. Following the schematic illustrated in Fig. 1(a), the colliding solitons have non-parallel relative velocities $\mathbf{v}_1, \mathbf{v}_2$, and $\mathbf{v}_3$, which means the collisions have both x and y components. In conditions of linear propagation, that is, for no previous exposure ($t = 0$), the input intensity pattern, the result of the coherent superposition of beams 1, 2, and 3 [Fig. 2(a)], diffracts at output [Fig. 2(b)]. Each single soliton diffracts from its initial 10 μm FHWM to 45 μm after propagating in the 1.8 mm long sample. As the space-charge buildup takes place ($t > 0$), self-focusing balances diffraction and a characteristic energy exchange occurs from soliton 1 to 2 and from 3 to 2 [Fig. 2(c) for $t = 150$ s]. The time dynamics of the self-focusing and energy transfer are reported in Fig. 2(d). The energy transfer amounts to an overall three-soliton fusion for $t > 70$ s and occurs along the x direction, i.e., the direction of the external bias electric field $\mathbf{E}_0$ (see Fig. 1). The final result of the three-soliton fusion is an intense solitonlike beam with approximately the same FWHM as each single colliding soliton [48]. Figures 2(e)–2(h) report the same experiment but now with the launch solitons at the vertices of a triangle that is inverted relative to the experiment in Figs. 2(a)–2(d) ($\mathbf{E}_0$ is kept the same). Results indicate an analogous final three-soliton fusion, while the actual final soliton position and velocity reflect the fact that energy exchange is now occurring from 2 to 1 and from 2 to 3. The final intense solitonlike beam appears to also form out of a resulting fusion of 1 and 3. Interestingly, solitons 1 and 3 do not

exchange energy, both in the case of Figs. 2(a)–2(d) and in that of Figs. 2(e)–2(h), in the absence of soliton 2 [41]. In other words, soliton 2 serves as the intermediate particle allowing their mutual coupling. Seen in terms of an optical computing element, the triple-soliton fusion amounts to a three-port logic AND gate, whereby light fuses into the final state reported in Figs. 2(c) and 2(g) only if all three colliding solitons are launched.

Figure 3 reports sample results of a three-soliton fusion in conditions of a collinear collision. Here, the three input solitons are launched with relative transverse velocities $\mathbf{v}_1 = -\mathbf{v}_3$, and $\mathbf{v}_2 = 0$, using the scheme illustrated in Fig. 1(c). The glass plate introduces a beam shift that causes the collision points inside the sample to be separated along z. Figures 3(a) and 3(b) report the input and output distribution for $t = 0$. In distinction to the noncollinear case, previous studies show that collinear collisions of three solitons without the glass plate manifest soliton chaos, not multisoliton fusion [45]. Introducing an appropriate glass plate in beam 1 [see Fig. 1(c)], the picture drastically changes: the output intensity distribution reported in Fig. 3(c) now shows a distinct and reproducible three-soliton fusion ($t > 190$ s). The result indicates that the passage from a soliton chaos behavior to three-soliton fusion is a direct consequence of the splitting of the triple collision into two distinct cascaded fusions, one fusing soliton 3 with soliton 2, and a second, fusing the result of the first fusion with soliton 1. As for the previous noncollinear case, the direction in which the fusion occurs depends on the orientation of the external bias field $\mathbf{E}_0$, that fixes the direction in which the nonlinear Raman-like component couples light nonreciprocally. Note that although the rotation of the glass plate may change the
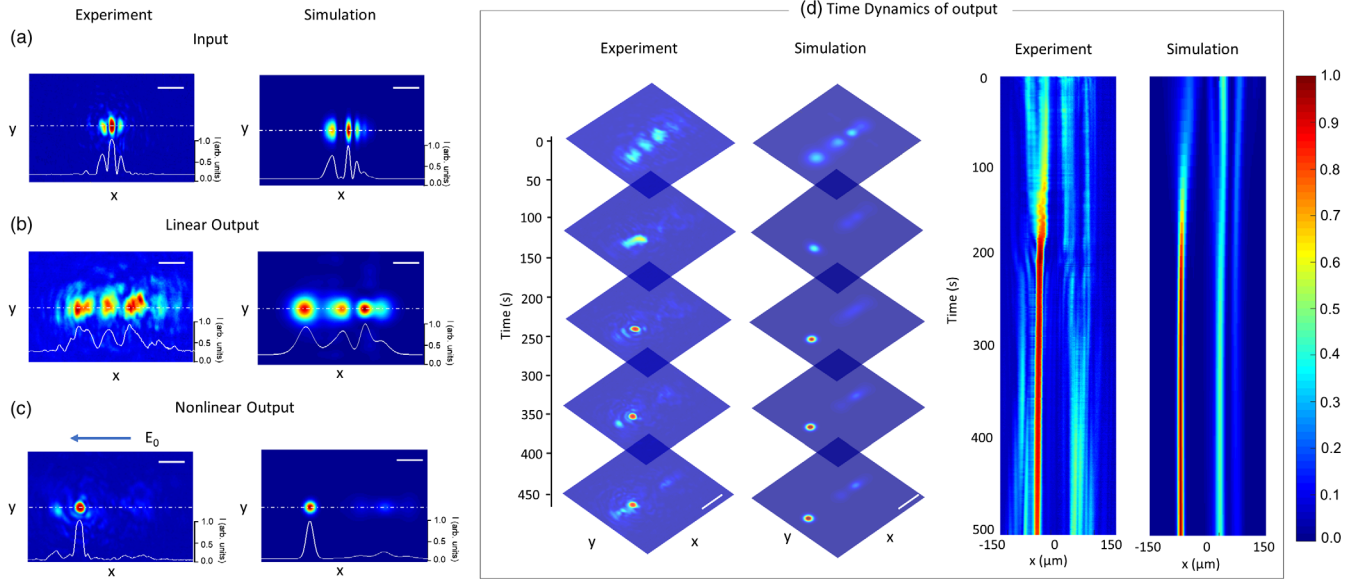
FIG. 3.   Intense waves from cascaded collinear three-soliton fusions. Experiment and simulation results of input (a), linear output (b), nonlinear output (c), and time dynamics (d) intensity distributions for cascaded soliton collisions. Panel (d) also contains the time evolution of the x profile of the output intensity distribution taken along the dashed line indicated in (c). The scale bar is for 50 μm.

relative phase of the colliding solitons, no observable difference was detected in the experiment due to this change, in agreement with the fact that the nonreciprocal Raman-like effect is insensitive to the relative phase between colliding solitons. The full time dynamics of the output intensity distribution as a function of exposure time t are reported in Fig. 3(d).

The time dynamics of the triple fusion are analyzed in Fig. 4 for the specific case of the collinear collision reported in Fig. 3. Output intensity distribution profiles reported in Fig. 4(a), for sample exposure times $t0$–$t3$, show a characteristic asymmetric shift in energy toward lower values of x, in the direction of $\mathbf{E}_0$. Nonreciprocal energy flow is evident monitoring the position of the center of mass of the distribution (intensity here plays formally the role of a mass density) versus exposure time t, as reported in Fig. 4(b) (see also Supplemental Material [47]). A second perspective is offered by the skewness parameter of the x intensity distribution, as reported in Fig. 4(c) (see the Supplemental Material [47]). The triple-soliton fusion is then found to have a transient asymmetry that coincides with the interval 190 s $< t <$ 350 s where a full fusion is observed [see Fig. 3(d)]. Evidence of an underlying transition in the wave dynamics is even more evident when analyzing the intensity autocorrelation (see Supplemental Material [47]), which abruptly decreases at $t^* \simeq 190$ s, as reported in Fig. 4(d). The autocorrelation at $r = 13$ μm ($\sim$ to the single soliton width) is found to drop to almost zero right after t^*, compared with its highest value 0.46 (1 being the maximum of the normalized form). The autocorrelation also reveals the transient nature of the phenomenon, as it starts to once again increase after

350 s. The picture is then that of a transient formation of a localized and intense wave, a transient feature that is a characteristic trait of rogue waves.

Comparing collinear and noncollinear collisions we see that if the dimensionality hosting the collision is larger than
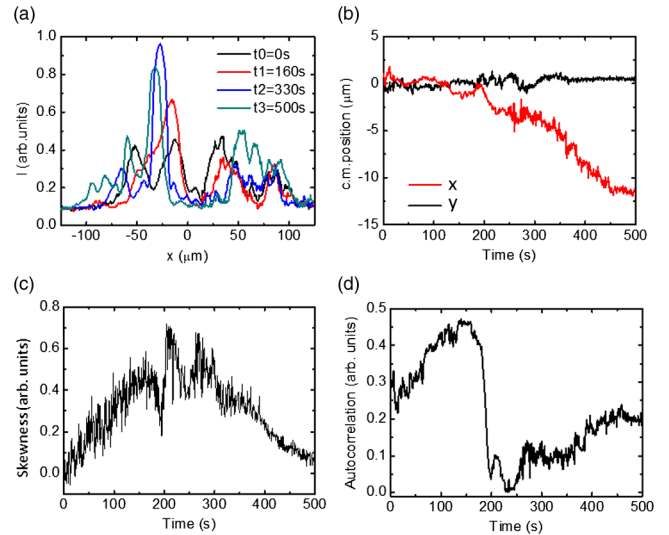

FIG. 4.   Transient nonreciprocal energy flow. (a) x profiles of output intensity distributions of cascaded solitons at different times. (b) Drift in the position of the optical center of mass vs time indicates an asymmetric overall beam deflection in the x direction. (c) Skewness of the x-profile distribution manifests a transient nature in the nonreciprocal energy flow. (d) Intensity autocorrelation vs time signals an accompanying transition at $t^* \simeq$ 190 s in the transverse spatial coherence of the patterns (see text and Supplemental Material [47]).

the dimensionality of the nonreciprocal interaction, conditions can be found in which multiple solitons fuse without chaotic behavior. In the noncollinear fusion analyzed in Fig. 2, this extra dimension is the second transverse direction in the $2 + 1$D propagation normal to the external field. In other systems, this extra dimension will be a subspace in which solitons collide with a degenerate velocity in the Raman subspace. For example, for guided light pulses, an extra dimension can be the different modes in a graded-index waveguide or the state of polarization, while for water waves colliding at sufficiently small angles, it can be the transverse axis. In the collinear case analyzed in Figs. 3 and 4, a cascade along propagation, the extra dimension is the propagation axis itself. Similar behavior is also expected for water waves and pulses in fibers, since in the case of a cascade, the multiple collisions are separated in time.

Summing up, we have performed comparative studies of the outcome of three-soliton collisions in photorefractive crystals, a system known to support solitons and rogue waves. Results bring us to conclude that three-soliton fusion is strongly dependent on the geometry and dimensionality of the collision. This sheds light on how dimensionality and nonreciprocal energy exchange affect the emergence of regular and chaotic soliton behavior, suggesting that extra dimensionality is at the heart of soliton rogue wave formation. Further studies will then aim at demonstrating the role of multiple soliton collisions in the development of out-of-equilibrium statistics, as done for extreme waves in semiconductor cavities [30].

[*]cindy.feifeixin@gmail.com

[1] Scientifc background on the Nobel Prize in Physics 2021, https://www.nobelprize.org/uploads/2021/10/sciback_fy_en_21.pdf (Nobel Committee for Physics, 2021).

[2] V. Tikhonenko, J. Christou, and B. Luther-Davies, Three Dimensional Bright Spatial Soliton Collision and Fusion in a Saturable Nonlinear Medium, Phys. Rev. Lett. 76, 2698 (1996).

[3] P. G. Drazin and R. S. Johnson, Solitons: An Introduction (Cambridge University Press, Cambridge, England, 1989).

[4] W. Królikowski, B. Luther-Davies, C. Denz, and T. Tschudi, Annihilation of photorefractive solitons, Opt. Lett. 23, 97 (1998).

[5] G. B. Whitham, Linear and Nonlinear Waves (Wiley, New York, 1974).

[6] Y. S. Kivshar and G. P. Agrawal, Optical Solitons from Fibers to Photonic Crystals (Elsevier Science, New York, 2003).

[7] Z. Chen, M. Segev, and D. N Christodoulides, Optical spatial solitons: Historical overview and recent advance, Rep. Prog. Phys. 75, 086401 (2012).

[8] J. H. V. Nguyen, P. Dyke, D. Luo, B. A. Malomed, and R. G. Hulet, Collisions of matter-wave solitons, Nat. Phys. 10, 918 (2014).

[9] H. Guo, M. Karpov, E. Lucas, A. Kordts, M. H. P. Pfeiffer, V. Brasch, G. Lihachev, V. E. Lobanov, M. L. Gorodetsky, and T. J. Kippenberg, Universal dynamics and deterministic switching of dissipative Kerr solitons in optical micro-resonators, Nat. Phys. 13, 94 (2017).

[10] Q. Fu, P. Wang, C. Huang, Y. V. Kartashov, L. Torner, V. V. Konotop, and F. Ye, Optical soliton formation controlled by angle twisting in photonic moiré lattices, Nat. Photonics 14, 663 (2020).

[11] B. Shen et al., Integrated turnkey soliton microcombs, Nature (London) 582, 365 (2020).

[12] W. He, M. Pang, D. Yeh, J. Huang, and P. S. J. Russell, Synthesis and dissociation of soliton molecules in parallel optical-soliton reactors, Light 10, 120 (2021).

[13] A. Armaroli, C. Conti, and F. Biancalana, Rogue solitons in optical fibers: A dynamical process in a complex energy landscape?, Optica 2, 497 (2015).

[14] P. Walczak, S. Randoux, and P. Suret, Optical Rogue Waves in Integrable Turbulence, Phys. Rev. Lett. 114, 143903 (2015).

[15] P. Suret, R. E. Koussaifi, A. Tikan, C. Evain, S. Randoux, C. Szwaj, and S. Bielawski, Single-shot observation of optical rogue waves in integrable turbulence using time microscopy, Nat. Commun. 7, 13136 (2016).

[16] J. M. Soto-Crespo, N. Devine, and N. Akhmediev, Integrable Turbulence and Rogue Waves: Breathers or Solitons?, Phys. Rev. Lett. 116, 103901 (2016).

[17] V. E. Zakharov, A. N. Pushkarev, V. F. Shvets, and V. V. Yan'kov, Soliton turbulence, JETP Lett., 48, 83 (1988).

[18] D. Pierangeli, F. Di Mei, G. Di Domenico, A. J. Agranat, C. Conti, and E. DelRe, Turbulent Transitions in Optical Wave Propagation, Phys. Rev. Lett. 117, 183902 (2016).

[19] N. Akhmediev and A. Ankiewicz, Multi-soliton complexes, Chaos 10, 600 (2000).

[20] P. Suret, A. Tikan, F. Bonnefoy et al., Nonlinear Spectral Synthesis of Soliton Gas in Deep-Water Surface Gravity Waves, Phys. Rev. Lett. 125, 264101 (2020).

[21] D. Pierangeli, A. Tavani, F. Di Mei, A. J. Agranat, C. Conti, and E. DelRe, Observation of replica symmetry breaking in disordered nonlinear wave propagation, Nat. Commun. 8, 1501 (2017).

[22] C. Conti and E. DelRe, Photonics and the Nobel Prize in physics, Nat. Photonics 16, 6 (2022).

[23] S. Randoux and P. Suret, Experimental evidence of extreme value statistics in Raman fiber lasers, Opt. Lett. 37, 500 (2012).

[24] N. Akhmediev, B. Kibler, and F. Baronio et al., Roadmap on optical rogue waves and extreme events, J. Opt. 18, 063001 (2016).

[25] D. R. Solli, C. Ropers P. Koonath, and B. Jalali, Optical rogue waves, Nature (London) 450, 1054 (2007).

[26] R. Driben and I. Babushkin, Accelerated rogue waves generated by soliton fusion at the advanced stage of supercontinuum formation in photonic-crystal fibers, Opt. Lett. 37, 5157 (2012).

[27] M. Onorato, S. Residori, U. Bortolozzoc, A. Montina, and F. T. Arecchi, Rogue waves and their generating mechanisms in different physical contexts, Phys. Rep. **528,** 47 (2013).

[28] J. M. Dudley, F. Dias, M. Erkintalo, and G. Genty, Instabilities, breathers and rogue waves in optics, Nat. Photonics **8,** 755 (2014).

[29] S. Birkholz, C. Brée, A. Demircan, and G. Steinmeyer, Predictability of Rogue Events, Phys. Rev. Lett. **114,** 213901 (2015).

[30] P. Walczak, C. Rimoldi, F. Gustave, L. Columbo, M. Brambilla, F. Prati, G. Tissoni, and S. Barland, Extreme events induced by collisions in a forced semiconductor laser, Opt. Lett. **42,** 3000 (2017).

[31] Z. Yang, W. Zhong, M. Belić, and Y. Zhang, Controllable optical rogue waves via nonlinearity management, Opt. Express **26,** 7587 (2018).

[32] D. Pierangeli, F. Di Mei, C. Conti, A. J. Agranat, and E. DelRe, Spatial Rogue Waves in Photorefractive Ferroelectrics, Phys. Rev. Lett. **115,** 093901 (2015).

[33] J. Peng, N. Tarasov, S. Sugavanam, and D. Churkin, Rogue waves generation via nonlinear soliton collision in multiple-soliton state of a mode-locked fiber laser, Opt. Exp. **24,** 24256 (2016).

[34] A. V. Slunyaev and E. N. Pelinovsky, Role of Multiple Soliton Interactions in the Generation of Rogue Waves: The Modified Korteweg–de Vries Framework, Phys. Rev. Lett. **117,** 214501 (2016).

[35] A. A. Gelash and D. S. Agafontsev, Strongly interacting soliton gas and formation of rogue waves, Phys. Rev. E **98,** 042210 (2018).

[36] F. Luan, D. V. Skryabin, A. V. Yulin, and J. C. Knight, Energy exchange between colliding solitons in photonic crystal fibers, Opt. Express **14,** 9844 (2006).

[37] F. J. Diaz-Otero, O. Guillán-Lorenzo, and L. Pedrosa-Rodriguez, Higher-order interaction-induced effects between strong dispersion-managed solitons with dissimilar powers, J. Opt. Soc. Am. B **34,** 12 (2017).

[38] X. Zhang, D. Pierangeli, C. Conti, D. Fan, and L. Zhang, Control of soliton self-frequency shift dynamics via airy soliton interaction, Opt. Express **26,** 32971 (2018).

[39] J. P. Gordon, Theory of the soliton self-frequency shift, Opt. Lett. **11,** 662 (1986).

[40] E. DelRe, B. Crosignani, and P. Di Porto, Photorefractive solitons and their underlying nonlocal physics, Prog. Opt. **53,** 153 (2009).

[41] F. Xin, M. Flammini, F. Di Mei, L. Falsi, D. Pierangeli, A. J. Agranat, and E. DelRe, Observation of extreme nonreciprocal wave amplification from single soliton-soliton collisions, Phys. Rev. A **100,** 043816 (2019).

[42] F. Xin, F. Di Mei, L. Falsi, D. Pierangeli, A. J. Agranat, and E. DelRe, Soliton Maxwell demons and long-tailed statistics in fluctuating optical fields, Opt. Lett. **45,** 648 (2020).

[43] M. Shih and M. Segev, Incoherent collisions between two-dimensional bright steady-state photorefractive spatial screening solitons, Opt. Lett. **21,** 1538 (1996).

[44] W. Królikowski and S. A. Holmstrom, Fusion and birth of spatial solitons upon collision, Opt. Lett. **22,** 369 (1997).

[45] F. Xin, F. Di Mei, L. Falsi, D. Pierangeli, A. J. Agranat, C. Conti, A. J. Agranat, and E. DelRe, Evidence of Chaotic Dynamics in Three-Soliton Collisions, Phys. Rev. Lett. **127,** 133901 (2021).

[46] E. DelRe, A. D'Ercole, and E. Palange, Mechanisms supporting long propagation regimes of photorefractive solitons, Phys. Rev. E **71,** 036610 (2005).

[47] See Supplemental Material at http://link.aps.org/supplemental/10.1103/PhysRevLett.129.043901 for simulation and data analysis methods.

[48] D. Pierangeli, G. Musarra, F. Di Mei, G. Di Domenico, A. J. Agranat, C. Conti, and E. DelRe, Enhancing optical extreme events through input wave disorder, Phys. Rev. A **94,** 063833 (2016).